Magnetoelectric Photocurrent Generated by Direct Interband Transitions in InGaAs/InAlAs Two-Dimensional Electron Gas

Junfeng Dai,[1] Hai-Zhou Lu,[1,2,*] C. L. Yang,[1,3] Shun-Qing Shen,[1,2] Fu-Chun Zhang,[1,2] and Xiaodong Cui[1,†]
[1]*Department of Physics, The University of Hong Kong, Pokfulam Road, Hong Kong, China*
[2]*Centre of Theoretical and Computational Physics, The University of Hong Kong, Pokfulam Road, Hong Kong, China*
[3]*Department of Physics, Sun Yat-Sen University, Guangzhou, Guangdong, China*
(Received 1 March 2010; published 14 June 2010)

We report the observation of magnetoelectric photocurrent generated via direct interband transitions in an InGaAs/InAlAs two-dimensional electron gas by a linearly polarized incident light. The electric current is proportional to the in-plane magnetic field, which unbalances the velocities of the photoexcited carriers with opposite spins and consequently generates the electric current from a hidden spin photocurrent. The spin photocurrent can be evaluated from the measured electric current, and the conversion coefficient of spin photocurrent to electric current is self-consistently estimated to be 10^{-3}–10^{-2} per Tesla. The observed light-polarization dependence of the electric current is well explained by a theoretical model which reveals the wave vector angle dependence of the photoexcited carrier density.

DOI: 10.1103/PhysRevLett.104.246601 PACS numbers: 72.25.Dc, 72.40.+w, 73.63.Hs, 78.67.De

Stimulated by the concept of nonmagnetic semiconductor spintronics devices [1], spin injection and detection by optical means have attracted much attention [2–17]. One way to generate spin current is to use linearly polarized optical excitations in bulk III–V semiconductors and quantum wells (QW) with asymmetric band structures induced by the strong spin-orbit coupling (SOC) [11–17]. The left and right circular components of the linearly polarized light generate the same amount of carriers with opposite spins and velocities, leading to a spin photocurrent accompanied by no electric current [18]. Because spin current carries neither net charge nor magnetization, it is necessary to convert the spin current to either electric current or magnetization for measurement [6–9,12,13,19–21]. An in-plane magnetic field may induce an imbalance of photoexcited carriers with opposite spins in the spin-split bands, resulting in an electric photocurrent. This field-induced conversion was systematically studied by intraband transitions involving abundant spin-dependent excitation and relaxation processes [16,17], and offered collateral evidence for pure spin currents. Since the induced charge current in the intraband transition is related to the scattering of carriers by phonon, impurity, or defect, it is difficult to use the method to estimate the field-induced conversion.

In this Letter we report a measurement of magnetoelectric photocurrent generated via direct interband transitions in an InGaAs/InAlAs two-dimensional electron gas by a linearly polarized light. The observed photocurrent and hence the hidden pure spin current, are several orders of magnitude larger than those via the intraband transition. The spin current generated thus appears promising as a step towards practical application. The simple picture of the direct interband transition enables us to have a reliable estimate of the pure spin current from the electric current, with the conversion rate found to be 10^{-3}–10^{-2} per Tesla. The estimated spin current is further confirmed by an anisotropic photocurrent induced Hall effect when the light sheds on the edge of the sample in the presence of a perpendicular magnetic field.

We start with discussions of our experimental setup, sample parameters, and the optical process. The experiment is carried out on the modulation doped $\mathrm{In}_x\mathrm{Ga}_{1-x}\mathrm{As}$/InAlAs QW grown along [001] direction, as shown in Fig. 1(a). The 40 nm InGaAs QW consists of graded indium composition from $x = 0.53$ to 0.59. The mobility and carrier (electron) density were measured as $\mu_m = 12\,000\ \mathrm{cm}^2 \cdot \mathrm{V}^{-1}\,\mathrm{s}^{-1}$ and $n_e = 2.2 \times 10^{12}\ \mathrm{cm}^{-2}$ at room temperatures by Hall measurements. The experiment setup is shown in Fig. 1(b). A 1050 μm long (L) and 50 μm wide strip of 2DEG channel along $[1\bar{1}0]$ and [110] directions was fabricated by standard photolithography and wet etching. The linearly polarized light at 1 mW normally sheds on the channel through a 10× objective lens. The electric photocurrent J_x passing through two terminals is monitored via the voltage drop V_x on a load resistor $R_{\mathrm{load}} = 3.9\ \mathrm{k}\Omega$ with a lock-in amplifier.

The band gap of 0.764 eV is extracted from the photomodulated differential reflectivity spectrum [22] as shown in Fig. 1(a). The pump source is a DFB packed laser diode at 1550 nm (0.80 eV), which excites the interband transition in the InGaAs channel. Since the photon energy is well above the band gap and the two lowest interband transition energies [marked by vertical dashed lines in Fig. 1(c)], the dominant optical absorption mechanism here is the direct interband transition, in which an electron in the valence band with the wave vector $\mathbf{k}$ absorbs a photon of energy $\hbar\omega$ and transits to the conduction band with the same wave vector.

In the analysis below we assume linear Rashba type spin-orbit coupling only, which leads to the two spin-split

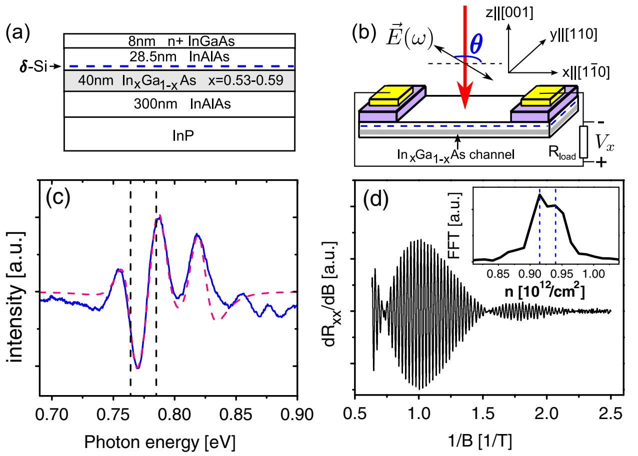

FIG. 1 (color online). (a) [001]-oriented InGaAs/InAlAs quantum well. (b) The experiment setup. A linearly polarized light (downward arrow) is normally incident with a polarization angle θ with respect to x axis. (c) Photomodulated differential reflectivity spectrum (blue solid curve) at 77 K with the pump light of a DPSS laser at 532 nm. Dashed curve is the spectrum analysis fitting curve [22]. The two lowest interband optical transitions below the photon energy (0.8 eV) are marked by the vertical dashed lines. (d) Shubnikov–de Haas (SdH) oscillation beating pattern of longitudinal magnetoresistance R_{xx} at $T = 2.5$ K. Inset: FFT spectrum of dR_{xx}/dB as a function of carrier concentration n, indicating two spin-split subbands (vertical dashed lines).

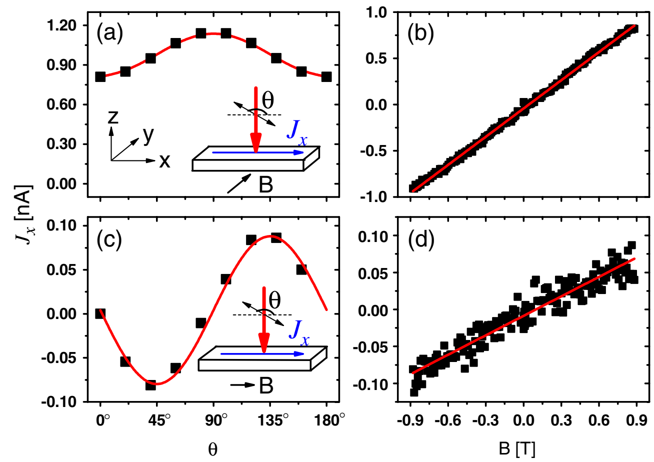

FIG. 2 (color online). Electric photocurrent J_x as a function of the polarization angle θ and in-plane magnetic fields B, along y axis [(a)–(b)], and along x axis [(c)–(d)], respectively. $B = 0.9$ T in (a) and (c). $\theta = 20°$ in (b), and $\theta = 120°$ in (d). The light beam with power of 1 mW from a DFB laser diode at 1550 nm is normally incident on the sample and the focused spot size is about 10 μm.

subbands, consistent with our experiment. The Shubnikov–de Hass (SdH) oscillation of the longitudinal magnetoresistance R_{xx} along the channel [23] is shown in Fig. 1(d). The SdH beating pattern of the derivative of R_{xx} and the corresponding fast Fourier transform (FFT) spectrum indicate the different carrier concentrations of the two subbands [24], as shown in the inset of Fig. 1(d). From these data, we estimate the Rashba coefficient to be $\alpha = 4.3 \times 10^{-12}$ eV $\cdot$ m [25].

Our main observations are summarized in Fig. 2, which shows the electric photocurrents J_x induced by the normally incident light as functions of in-plane magnetic fields $\mathbf{B}$ along the y direction [(a)–(b)] and along the x direction [(c)–(d)], respectively. J_x is essentially zero at $\mathbf{B} = 0$, and is linearly proportional to $\mathbf{B}$. J_x increases linearly with the light intensity up to the maximum laser power of 10 mW. Furthermore, J_x has a clear light-polarization dependence, as shown in Figs. 2(a) and 2(c). The relation between the electric photocurrent, magnetic fields, and polarization angle θ can be summarized by

$$J_x(B_x, B_y, \theta) = c_0 B_y + c_y B_y \cos 2\theta + c_x B_x \sin 2\theta, \quad (1)$$

where $c_{0,x,y}$ are all proportional to the light intensity. The first term describes the polarization-independent part, and is a dominant contribution to the magnetoelectric effect, as we can see from Fig. 2. The second and third terms represent the light-polarization dependences of the magnetoelectric effect, which are about 1 order in magnitude smaller than the first term, and are consistent with the C_{2v} crystal symmetry of the zinc blende QW grown along [001] direction [17,26].

Below we shall first present a simple picture to qualitatively explain the magnetic-field-induced conversion from the pure spin current to the electric photocurrent. The picture [Figs. 3(a) and 3(b)] can be illustrated by a valence band $|v, \mathbf{k}\rangle$ and two spin-split conduction subbands $|c = \pm, \mathbf{k}\rangle$ with the band dispersions

$$E_{\pm}(\mathbf{k}) = \frac{\hbar^2}{2m^*}k^2 \pm \sqrt{(\alpha k_y + h_x)^2 + (\alpha k_x - h_y)^2}, \quad (2)$$

where $k_{x,y}$ are the in-plane wave vectors, $k^2 = k_x^2 + k_y^2$, $\sigma_{x,y}$ are the Pauli matrices, and $h_{x,y}$ denote the Zeeman energies of the in-plane magnetic fields. In $\mathbf{k}$ space, the states involved in the interband transition form the constant energy contours which, in the absence of magnetic fields, are perfect concentric circles split by the SOC [Fig. 3(a)]. Because of the time-reversal symmetry, for each state on a constant energy contour, there always exists another state with opposite velocity and spin; therefore they cancel one another to give no electric photocurrent, but a nonzero spin photocurrent [11,14,15,18]. According to the above $E_{\pm}(\mathbf{k})$, applying in-plane fields will lead to the Zeeman shifts of the bands and distort the constant energy contours to Fig. 3(b). This shift then breaks the balance of both velocities and photoexcited carrier density on the constant energy contours and leads to a finite electric photocurrent. Besides the Zeeman effect, a shift can also be induced by the diamagnetic mechanism [27,28], but the consequence should be qualitatively similar.

Now we use a theoretical model to further explain the experimental observation in Eq. (1). The electric photocurrent density j_x can be calculated by summing the velocities of the photoexcited carriers $j_x = -e\sum_{c,v,\mathbf{k}} \rho_{cv,\mathbf{k}} v^x_{c\mathbf{k}}$, where $-e$ is the electron charge, $\rho_{cv,\mathbf{k}}$ is the carrier density, and $v^x_{c\mathbf{k}}$ denotes the x-axis velocity of $|c, \mathbf{k}\rangle$. For convenience, the summation over $\mathbf{k}$ can be rewritten into an integral in polar coordinates

$$j_x = \frac{-e}{(2\pi)^2} \sum_{c,v} \int_0^{2\pi} d\varphi \int_0^\infty kdk\delta(k - k_{cv}) \rho_{cv,\mathbf{k}} v^x_{c\mathbf{k}}, \quad (3)$$

where the wave vector angle φ is defined as $\tan\varphi \equiv k_y/k_x$, k_{cv} are the magnitudes of wave vectors on a constant energy contour. For small magnetic fields, we can expand the velocity $v^x_{\pm\mathbf{k}} \equiv (1/\hbar)\partial E_\pm(\mathbf{k})/\partial k_x$ up to the linear order of the Zeeman energy $h_{x(y)}$ along $x(y)$ axis as

$$v^x_{\pm\mathbf{k}} \simeq \left(\frac{\hbar}{m^*} k \pm \frac{\alpha}{\hbar}\right) \cos\varphi \mp \frac{\sin 2\varphi}{2\hbar k} h_x \mp \frac{\sin^2\varphi}{\hbar k} h_y. \quad (4)$$

Similar to the second-order nonlinear optical susceptibility, $\rho_{cv,\mathbf{k}}$ in Eq. (3) can be evaluated by the density matrix formalism [11]. Simply speaking, as a second-order optical quantity, $\rho_{cv,\mathbf{k}}$ should be proportional to $|\mathbf{E} \cdot \mathbf{r}_{cv}|^2$ where $\mathbf{E} = E_0(\cos\theta, \sin\theta)$ is the polarization electric field vector and $\mathbf{r}_{cv} = (x_{cv}, y_{cv})$ is the expectation value of position operator between conduction and valence bands. Then $\rho_{cv,\mathbf{k}}$ turns out to be well described by the form

$$\rho_{cv,\mathbf{k}} = \rho^0_{cv} + \rho^{\cos}_{cv} \cos 2\varphi \cos 2\theta + \rho^{\sin}_{cv} \sin 2\varphi \sin 2\theta. \quad (5)$$

As shown in Figs. 3(c)–3(e), $\rho_{cv,\mathbf{k}}$ has an anisotropic φ dependence. Putting the above $\rho_{cv,\mathbf{k}}$ and $v^x_{\pm\mathbf{k}}$ into Eq. (3) immediately yields a current density in the same form as Eq. (1) [29]. For example, one can check that the first term of $\rho_{cv,\mathbf{k}}$ and the last term of $v^x_{c\mathbf{k}}$ gives the $c_0 B_y$ term of Eq. (1). Above we neglect the hole contribution from the valence bands, as the lifetime and spin relaxation time of holes in the n-type well are much shorter than those of electrons.

The theoretical model allows us to estimate the magnitude of the zero-field pure spin photocurrent from the measured field-induced electric photocurrent. The zero-field spin velocities are defined as (flowing along x, polarized along x and y axes) $(s_x^{x/y})_{\pm\mathbf{k}} \equiv \langle \pm, \mathbf{k}|\frac{1}{2}\{\hat{v}_x, \hat{\sigma}_{x/y}\}|\pm, \mathbf{k}\rangle$, specifically, $(s^x_x)_{\pm\mathbf{k}} = \pm\frac{\hbar}{2m^*} k \sin 2\varphi$ and $(s^y_x)_{\pm\mathbf{k}} = (\mp \frac{\hbar}{m^*} k \cos^2\varphi - \frac{\alpha}{\hbar})$. The spin currents can be evaluated by replacing $v^x_{c\mathbf{k}}$ in Eq. (3) with $(s_x^{x/y})_{c\mathbf{k}}$. Note that the zero-field spin velocity $\propto \hbar k/m^*$ and the magnetic-field-induced electron velocity variation $\propto h_\mu/\hbar k$, their ratio $\frac{\hbar^2 k^2}{2m^*}/h_\mu$ can be employed to approximate the ratio of the zero-field pure spin current over the field-induced electric current in strength. This ratio could be further interpreted as "kinetic energy over Zeeman energy." The kinetic energy can be estimated to be about 10^{-2}–10^{-1} eV from the carrier density $n_e = 0.93 \times 10^{12}/\text{cm}^2$, and the Zeeman energy h_μ is about 1.2×10^{-4} eV/Tesla (Landé g factor ≈ -4 [23,30]). The field-induced electric photocurrent density of about 10^{-5} A/m can be found from the measured J_x in Fig. 2. Summarizing above gives a magnitude of the spin photocurrent density about 10^{-3}–10^{-2} A/m for a 1 mW incident light, and a conversion coefficient from spin photocurrent to field-induced electric photocurrent about 10^{-3}–10^{-2} per Tesla. In the above analysis, we replace the unit $\hbar/2$ of the spin current with $-e$ for direct comparison with the electric current.

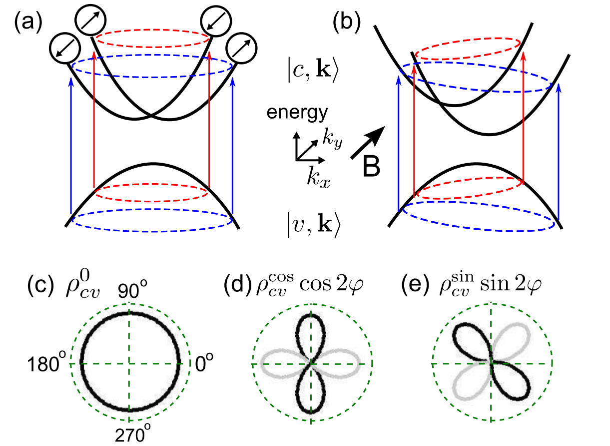

FIG. 3 (color online). Schematic description of direct optical excitations from a valence band $|v, \mathbf{k}\rangle$ to the spin-split conduction bands $|c = \pm, \mathbf{k}\rangle$ at magnetic field $\vec{B} = 0$ (a) and $\vec{B}$ along y axis (b). Dashed rings indicate the constant energy contours of photoexcited conduction electrons, which are symmetric at $\vec{B} = 0$ and shifted along k_y (k_x) in the presence of a magnetic field B_x (B_y). The circled arrows denote the relative spin orientations which are in-plane and perpendicular to wave vector. [(c)–(e)] Wave vector angle (φ) dependence of photoexcited carrier density $\rho_{cv,\mathbf{k}}$ in Eq. (5) at $\vec{B} = 0$. Only the results on one constant energy contour are shown. Dark (light) curves represent positive (negative) values. ρ^0_{cv} is always larger than $\rho^{\cos/\sin}_{cv}$ terms.

In what follows, we shall describe a second method to estimate the spin photocurrent by employing a photoexcited Hall measurement, in which the optical pumping acts like a current source in the usual Hall measurement. Our finding is consistent with and further supports the estimation of the spin current from the magnetoelectric photocurrent. We apply an out-of-plane magnetic field B_z, and scan the light spot across the channel along y axis (Fig. 4). The light spot may generate photocurrents diffusing out of the spot edge in all directions with the identical charge current density j_0 (note that j_0 is completely different from the field-induced electric photocurrent in Fig. 2). When the spot is right focused on one edge of the sample, the anisotropic diffusion leads to a net current Dj_0 ($D = 10$ μm denotes the spot diameter) normal to the edge and consequently produces a Hall voltage along x direction under the magnetic field B_z. Figure 4 shows V_x as a function of the spot position y_{spot} (the scanning path is marked by the dotted line). The positive and negative peaks

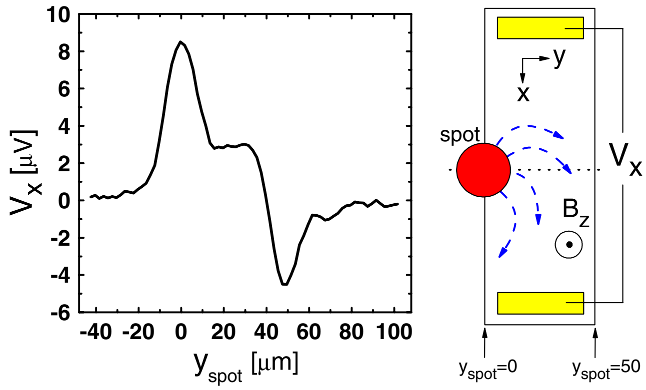

FIG. 4 (color online). Hall voltage V_x as a function of the spot position $y_{\rm spot}$, in the presence of out-of-plane magnetic fields B_z ($=0.15$ T). The right sketch shows the experimental setup, where a light is shed on the spot at edge of the sample. The scanning path of $y_{\rm spot}$ is marked by the horizontal dotted line. The dashed arrows indicate the Hall current trajectory induced by B_z. The bar size is $50 \times 1050\ \mu\text{m}^2$, $\theta = 0$. The plateau at $y_{\rm spot} = 20$ is due to the in-plane magnetic field ($B_y = 0.86$ T) induced electric current as in Fig. 2.

correspond to where the light spot is located at the left and right edges of the channel, respectively. If the spot is away from the edges, the diffusion of the photocurrent is isotropic and consequently the Hall voltage vanishes. The plateau in Fig. 4 is attributed to the in-plane magnetic field as those in Fig. 2. At the edges, Dj_0 is related to V_x by a transverse Hall resistivity $\rho_{xy} \approx 2B_z/\pi e n_e$, then $j_0 \approx \pi e n_e V_x/2DB_z \approx 2.4 \times 10^{-2}$ A/m at the peaks ($|V_x| \approx 6.5\ \mu$V) in Fig. 4. Roughly speaking, j_0 can be viewed as $j_\uparrow + j_\downarrow$ while the spin current as $j_\uparrow - j_\downarrow$, and $(j_\uparrow - j_\downarrow)/(j_\uparrow + j_\downarrow) \sim \Delta n/\bar{n}$. With $\Delta n/\bar{n} \approx 0.027$ [Fig. 1(d)], the spin photocurrent is estimated about 0.7×10^{-3} A/m, and agrees with the low bound by the magnetoelectric effect. Furthermore, j_0 can also be evaluated from the conversion of the light power into the photocurrent. If the sample reflectance of 0.3, photon-carrier yield of 30%, and the absorption coefficient of $9 \times 10^3\ \text{cm}^{-1}$ are assumed, the spin current density is found to be around 10^{-2} A/m, consistent with the high bound obtained by the magnetoelectric effect. Comparing the above spin current density range (0.7×10^{-3}–10^{-2} A/m) with the electric photocurrent signal owing to B_y (the plateau in Fig. 4, note when $\theta = 0$, B_z, and B_y induced currents just add up to one another), one could estimate the conversion coefficient of spin photocurrent to field-induced electric photocurrent at 10^{-3}–1.7×10^{-2} per Tesla, in good agreement with those by the magnetoelectric effect.

In summary, we have observed magnetic-field-induced electric photocurrent via the direct interband optical absorption. We have estimated the conversion coefficient of spin photocurrent to field-induced electric photocurrent to be 10^{-3}–10^{-2} per Tesla. Our experiment demonstrates that optical injection via the direct interband transition is a promising means to generate and detect spin photocurrent, as well as a reference for future evaluation of pure spin currents. This should stimulate further experiments to study nonmagnetic spintronics towards its practical applications.

This work was supported by the Research Grant Council of Hong Kong under Grants No. HKU 7013/08P, No. HKU 7041/07P, No. HKU 10/CRF/08, and Hong Kong UGC Grant No. AOE/P-04/08.

*luhaizhou@gmail.com
†xdcui@hku.hk

[1] D. Awschalom and M. Flatte, Nature Phys. **3**, 153 (2007).
[2] S. D. Ganichev *et al.*, Nature (London) **417**, 153 (2002).
[3] S. D. Ganichev and W. Prettl, J. Phys. Condens. Matter **15**, R935 (2003).
[4] R. D. R. Bhat and J. E. Sipe, Phys. Rev. Lett. **85**, 5432 (2000).
[5] J. Hübner *et al.*, Phys. Rev. Lett. **90**, 216601 (2003).
[6] M. J. Stevens *et al.*, Phys. Rev. Lett. **90**, 136603 (2003).
[7] Y. K. Kato *et al.*, Science **306**, 1910 (2004).
[8] J. Wunderlich *et al.*, Phys. Rev. Lett. **94**, 047204 (2005).
[9] H. Zhao *et al.*, Phys. Rev. Lett. **96**, 246601 (2006).
[10] X. W. He *et al.*, Phys. Rev. Lett. **101**, 147402 (2008).
[11] R. D. R. Bhat *et al.*, Phys. Rev. Lett. **94**, 096603 (2005).
[12] H. Zhao *et al.*, Phys. Rev. B **72**, 201302(R) (2005).
[13] X. D. Cui *et al.*, Appl. Phys. Lett. **90**, 242115 (2007).
[14] J. Li *et al.*, Appl. Phys. Lett. **88**, 162105 (2006).
[15] B. Zhou and S. Q. Shen, Phys. Rev. B **75**, 045339 (2007).
[16] S. D. Ganichev *et al.*, Nature Phys. **2**, 609 (2006).
[17] V. V. Bel'kov *et al.*, J. Phys. Condens. Matter **17**, 3405 (2005).
[18] S. A. Tarasenko *et al.*, JETP Lett. **81**, 231 (2005).
[19] S. O. Valenzuela *et al.*, Nature (London) **442**, 176 (2006).
[20] I. Appelbaum *et al.*, Nature (London) **447**, 295 (2007).
[21] J. Wang *et al.*, Phys. Rev. Lett. **100**, 086603 (2008).
[22] D. E. Aspnes, in *Handbook on Semiconductors*, edited by T. S. Moss (North-Holland, New York, 1980), Vol. 2, p. 109.
[23] J. Nitta *et al.*, Phys. Rev. Lett. **78**, 1335 (1997).
[24] G. Engels *et al.*, Phys. Rev. B **55**, R1958 (1997).
[25] In the estimation [24], $\alpha = \frac{\Delta n \hbar^2}{m^*}\sqrt{\frac{\pi}{2(\bar{n}-\Delta n)}}$, where $\bar{n} = 0.93 \times 10^{12}/\text{cm}^2$ and $\Delta n = 0.025 \times 10^{12}/\text{cm}^2$ are the average value and the difference of the two carrier concentrations extracted in the inset of Fig. 1(d), and the effective mass $m^* = 0.04 m_e$ is assumed.
[26] Our theoretical model assumes $C_{\infty v}$ symmetry, which can be generalized to C_{2v} by considering anisotropic Rashba coefficients along x and y axes. For $C_{\infty v}$, $|c_x| = |c_y|$ in Eq. (1), which does not hold for C_{2v}.
[27] F. Stern and W. E. Howard, Phys. Rev. **163**, 816 (1967).
[28] A. A. Gorbatsevich *et al.*, JETP Lett. **57**, 580 (1993).
[29] Under the same principle of the φ dependence, the variation of $\rho_{cv,\mathbf{k}}$ upon applying B field also leads to a contribution to J_x of the same order as those from $v_{c\mathbf{k}}$.
[30] T. P. Smith III and F. F. Fang, Phys. Rev. B **35**, 7729 (1987).